RESEARCH ARTICLE | JUNE 20 2023

Atomic scale mechanism of β to γ phase transformation in gallium oxide \odot

Hsien-Lien Huang ■ ⑥ ; Jared M. Johnson ⑥ ; Christopher Chae; Alexander Senckowski ⑥ ; Man Hoi Wong ⑥ ; Jinwoo Hwang ■ ⑥

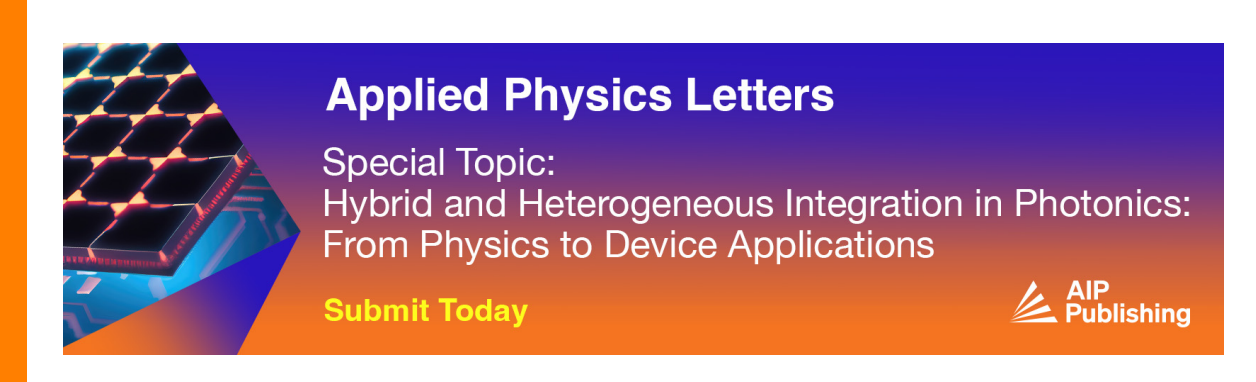


Appl. Phys. Lett. 122, 251602 (2023) https://doi.org/10.1063/5.0156009





CrossMark





Atomic scale mechanism of β to γ phase transformation in gallium oxide 😥

Cite as: Appl. Phys. Lett. 122, 251602 (2023); doi: 10.1063/5.0156009 Submitted: 25 April 2023 · Accepted: 1 June 2023 ·







Published Online: 20 June 2023

Hsien-Lien Huang,^{1,a)} 🕞 Jared M. Johnson,¹ 🅞 Christopher Chae,¹ Alexander Senckowski,² 🕞 Man Hoi Wong,² 🕞 and Jinwoo Hwang^{1,a)} (b)





AFFILIATIONS

- 1 Department of Materials Science and Engineering, The Ohio State University, Columbus, Ohio 43210, USA
- ²Department of Electrical and Computer Engineering, University of Massachusetts Lowell, Lowell, Massachusetts 01854, USA

ABSTRACT

We report the detailed mechanism behind the β to γ phase transformation in Sn-doped and Si-implanted Ga₂O₃ that we determined based on the direct observation of the atomic scale structure using scanning transmission electron microscopy (STEM). Quantitative analysis of the STEM images revealed that the high concentration of impurity atoms favored the formation of interstitial-divacancy complexes, which then leads to the secondary relaxation that creates additional interstitial atoms and cation vacancies, resulting in a local structure that closely resembles γ -Ga₂O₃. We explain the mechanism of how the impurity atoms facilitate the transformation, as well as the detailed sequence of the local y phase transformation. The findings here offer an insight on how the lattice respond to the external stimuli, such as doping and strain, and transform into different structures, which is important for advancing Ga₂O₃ but also a variety of low symmetry crystals and oxides with multiple polymorphs.

Published under an exclusive license by AIP Publishing. https://doi.org/10.1063/5.0156009

Beta-gallium oxide (β-Ga₂O₃) has emerged as the next generation ultrawide bandgap (UWBG) semiconductor material, and it has extensively been studied recently as a potential candidate for high power electronics and deep ultraviolet photodetector applications. I Its main advantages include a high breakdown electric field strength of 8 MV/cm, a bandgap of ~4.8 eV, 10 and optical transparency into the ultraviolet region. Utilizing the properties of β -Ga₂O₃ requires understanding and controlling defects, especially the point defects.¹² These defects can be induced, for example, by doping ¹³ and alloying, ¹⁴ and they may result in various alterations of the local atomic structure, including the formation of defect complexes15 that may have a wide range of electronic properties, which can critically influence the macroscopic character of the material. Another important aspect of β - Ga_2O_3 thin film growth is the formation of local γ phase, which has been observed in various types of epitaxial β-Ga₂O₃ films. For example, the formation of γ-Ga₂O₃ was experimentally observed in the films grown on different substrates (sapphire, 16-19 MgAl₂O₄, 20-25 and MgO²⁶) and with various growth methods, such as mist chemical vapor deposition (mist-CVD),^{23,24,27} pulsed laser deposition (PLD), 16,18,21,22 molecular beam epitaxy (MBE), 24,25 metal organic vapor phase epitaxy (MOVPE),²⁸ sol-gel,^{17,29} hydrothermal,^{30–35} sonochemical, 36 and solvothermal $^{37-45}$ processes. The formation of γ - Ga₂O₃ has also been observed in alloys and heterostructures, including γ -(Al_xGa_{1-x})₂O₃ thin films^{27,46-48} and Ga₂O₃ nanostructures, such as quantum dots, 34,49,50 nanorods, 51 and nanoparticles. 52

γ-Ga₂O₃ itself has its own unique characteristics, such as the tunable photoluminescence ^{39,50,53,54} and different band gaps, ^{27,46–48} which can be the subjects of separate research. However, for the β -Ga₂O₃ thin film growth, it is important to understand the exact mechanism of the unintended formation of γ phase, which has remained unclear. In general, γ-Ga₂O₃ is considered metastable, which intrinsically contains some amounts of disorder and local distortion due to both the ratio of tetrahedral to octahedral Ga sites and ratio of spinel to nonspinel sites.^{55–57} Density functional theory calculations suggest that the monoclinic β -phase (C2/m) is the most stable and that the γ -phase 8 is metastable. The calculated thermodynamic stability of the polymorphs is in the following order: $\beta < \varepsilon < \alpha < \delta < \gamma$, which assumes an equilibrium growth condition. Interestingly, however, in non-equilibrium conditions, such as in thin film growth of β - Ga_2O_3 , the local formation of γ - Ga_2O_3 , which is the least stable phase, has been shown to be prevalent, while the formation of the other phases $(\alpha, \varepsilon, \text{ and } \delta)$ was not commonly observed in the previous works. While the exact reason for this γ-Ga₂O₃ formation has been unclear, and the fact that the γ -phase tend to become more stable

^{a)}Authors to whom correspondence should be addressed: huang.3527@osu.edu and hwang.458@osu.edu

when β -Ga₂O₃ is either doped^{22,60} or alloyed^{27,46–48} suggests that there may be an atomic scale mechanism of point defects somehow facilitating the formation of γ phase. Surface diffusion during the film growth may also be related to the formation of γ phase.⁴⁸

Previous studies have suggested various factors that potentially influencing the γ phase formation within β -Ga₂O₃. For example, the coexistence of β and γ phases in homoepitaxial⁶¹ and heteroepitaxial⁶⁰ films suggested that the metastable γ phase can be a kinetically preferred configuration^{60,62} that depends on the processing parameters, for example, doping,⁶⁰ ion implantation,^{63,64} temperature,^{45,62,65} and impurity concentrations.⁶¹ Other factors, such as strain,^{64,66} intrinsic vacancies,⁵⁵ and the structural similarity of [010] β -Ga₂O₃ and [110] γ -Ga₂O₃,⁶³ have also been considered potentially contributing to the γ phase transformation. Transmission electron microscopy (TEM) studies on γ -Ga₂O₃ nanocrystals⁴⁵ and thin films ^{56,60,63,65} have also been performed to understand the β to γ phase transition. Nevertheless, the atomic scale mechanism of the β to γ phase transformation has not been experimentally confirmed, leaving the exact nature of the transition largely in question.

In this Letter, we present an atomic scale mechanism of β to γ phase Ga₂O₃ transformation directly observed using scanning transmission electron microscopy (STEM). We show that the previously observed interstitial-divacancy complex, 15,67-69 when existing in high concentration, can lead to secondary relaxation of the lattice which creates additional interstitial atoms and vacancies nearby, resulting in a local structure that closely resemble γ -Ga₂O₃. We point out that this atomic scale relaxation process is essentially the β to γ phase transformation. This mechanism of γ phase transformation was observed in β-Ga₂O₃ doped with different dopants (Sn and Si) and different doping methods (bulk doping and ion implantation), which suggests that the mechanism can be generally applicable in various synthesis and growth of β -Ga₂O₃. Our work, therefore, shows the detailed structure of point defects (0-D defects) and their complexes and how they can further relax the local structure to form local γ phase phases (3D defects), providing a way to understand the phase transformation in Ga₂O₃ under external stimuli, such as doping, alloying, ion implantation, and strain accumulation.

First, we performed the STEM investigation on the interstitial defects in ($\overline{2}01$) Sn-doped β -Ga₂O₃ bulk crystals. The samples were fabricated by edge-defined, film-fed growth 70,71 with the doping concentration of $8.5 \times 10^{18} \, \mathrm{cm}^{-3}$ and carrier concentration of $8.2 \times 10^{18} \, \mathrm{cm}^{-3}$. The TEM foils were prepared using a dual beam focused ion beam (FIB). We then used a 500 V ion mill (Fischione Nanomill) to further thin the foil and clean the surface. STEM was performed using the aberration-corrected Thermo Fisher Scientific Themis STEM (Cs₃ = 0.002 mm, Cs₅ = 1.0 mm, α = 20.0 mrad, 300 kV). β -Ga₂O₃ is a monoclinic crystal structure, comprising of two inequivalent sites with tetrahedral (Ga1) and octahedral (Ga2) coordination, and three inequivalent O sites with threefold (O1, O2) and fourfold (O_3) coordination. Figure 1(a) shows a [010] β -Ga₂O₃ crystal that includes five cation interstitial sites predicted by theoretical calculations $(i_{a-c})^{68,69}$ and experimental observation $(i_{a-e})^{15}$. The high angle annular dark field (HAADF) STEM image of Sn-doped β-Ga₂O₃ is shown in Fig. 1(b), revealing a defect-free region (inset) with high intensity from Ga columns and much weaker intensity from O columns as their atomic numbers dominate the contrast in the image. In contrast to the defect-free region, a significant amount of interstitial

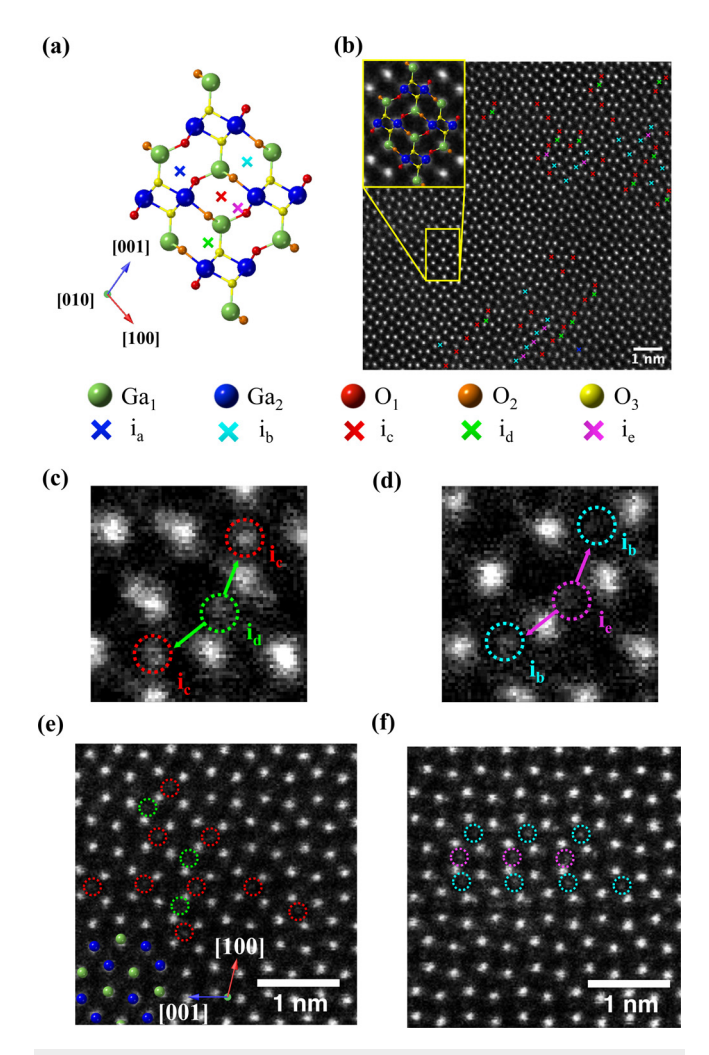


FIG. 1. (a) Crystal structure of β-Ga $_2$ O $_3$ along the [010]_m direction with five possible interstitial sites (i_{a-e}). Colors of atoms represent the different cation and oxygen sites, and the color of X marks represents different interstitial sites. (b) HAADF STEM image of Sn-doped [010] β-Ga $_2$ O $_3$ bulk crystal from a defect free region (inset) and other areas with clustered interstitial defects. Magnified regions from image in (b) reveal the combination of interstitial atoms with the configurations of (c) $2i_c$ - i_d and (d) $2i_b$ - i_e observed in Si implanted β-Ga $_2$ O $_3$ with the average Si concentration of 10^{20} cm $^{-3}$. Images [Figs. 1(b)–1(d)] were acquired from the same sample that we used to produce the images in Johnson *et al.* ¹⁵ However, the current images show different areas of the sample.

atoms (X marks) can be seen in other regions of Fig. 1(b), especially at i_b , i_c , i_d , and i_e sites. As shown in the figure, these interstitial atoms tend to cluster at the nanometer scale volume. The number of columns with observable point defects was approximately 80 for the Sn-doped β -Ga₂O₃ [Fig. 1(b)]. By analyzing visible interstitials within the field of view, the total concentration of defect complexes (Sn vs Ga) was calculated to be around 1.32×10^{20} and 2.63×10^{20} cm⁻³ which are close to the reported defect density. The More importantly, we observed a compelling trend of i_d interstitials accompanied by two adjacent i_c [Fig. 1(c)] and i_e interstitials accompanied by two i_b interstitials, respectively

[Fig. 1(d)]. Similarly, the same type of i_c – i_d and i_b – i_e pairings, as well as their local clustering was also observed in Si implanted β -Ga₂O₃ with the implantation concentration of 10^{20} cm⁻³, as shown in Figs. 1(e) and 1(f).

Our previous study using a quantitative analysis of atomic column intensities in HAADF images¹⁵ revealed that i_b and i_c interstitials involve two Ga vacancies nearby, forming an interstitial-divacancy complexes that have been predicted by DFT calculations.⁶⁸ The fact that the current work, shown in Fig. 1, further revealed the convincing evidence of i_c-i_d and i_b-i_e pairings suggests that there may be a secondary atomic scale relaxation occurring when multiple interstitialdivacancy complexes are adjacent to each other due to clustering. To understand the details of the relaxation, we performed the quantitative analysis of the column intensities in the regions where we observed clustered ib-ie interstitial atoms. Using the quantitative analysis of atomic column intensities, 15 we have detected measurable amounts of cation vacancies within those regions. Figure 2(a) is an example image showing presence of vacancies nearby i_c and i_d atoms. Since the atomic column intensities are normalized by the incident beam intensity, 7 the column intensity can directly indicate how many atoms are within the column. Similarly, the decrease in the column intensity indicates the presence of the vacancies within the column. ¹⁵ We drew the line profiles of the absolute column intensities along the colored (orange, blue, green, and purple) lines and averaged them over 20 different areas similar to the image in Fig. 2(a), which are shown in Figs. 2(b) and 2(c). First, the intensity profile across the orange line in Fig. 2(a) reveals almost an equal intensity for both Ga2 columns [Fig. 2(b)] that

matches the column intensities of regular (defect free) Ga2 columns, indicating these are regular Ga2 columns and contain no additional vacancies. On the other hand, the intensity profile across the blue line in Fig. 2(a) displays a decrease in intensity of the right Ga₂ column [blue arrow in Fig. 2(b)], suggesting that the column contains some amount of cation vacancies. The intensity of the right column in the blue line profile is in fact comparable to the column intensities in green and purple profiles [Fig. 2(c)], which we know contain vacancies since those columns are part of the interstitial-divacancy complexes (2V_{Ga}¹-Ga_i^c) that we identified in our previous work.¹⁵ The effect of vacancies to the column intensities in HAADF images was also confirmed using multislice image simulations⁷³ using the frozen phonon model (see the supplementary material for details). Based on the experimental result, we made a model of the local region corresponding to the area in Fig. 2(a) to show the locations of the vacancies (circles with V) as well as the iand id interstitials, as shown in Fig. 2(d). The same analysis was performed for the structure involving i_b and i_e interstitials [Fig. 2(e)], which resulted in the line profiles [Figs. 2(f) and 2(g)] and the structure with the vacancy distribution shown in Fig. 2(h). The analysis shows the equivalent trend as the case of ic and id interstitials.

Based on the atomic scale characterization of HAADF-STEM interstitial and neighboring column intensities, we developed the formation mechanism for the interstitial complexes, $2i_c$ – i_d and $2i_b$ – i_e and how they convert to the structure of γ phase inclusion. Previous studies have shown the formation of point defect complexes, $2V_{Ga}^1$ – $Ga_i^{b,c}$, which are resulted from the migration mechanism of cation vacancies that occupy the energetically favorable tetrahedral Ga_1 site. 68,69 The

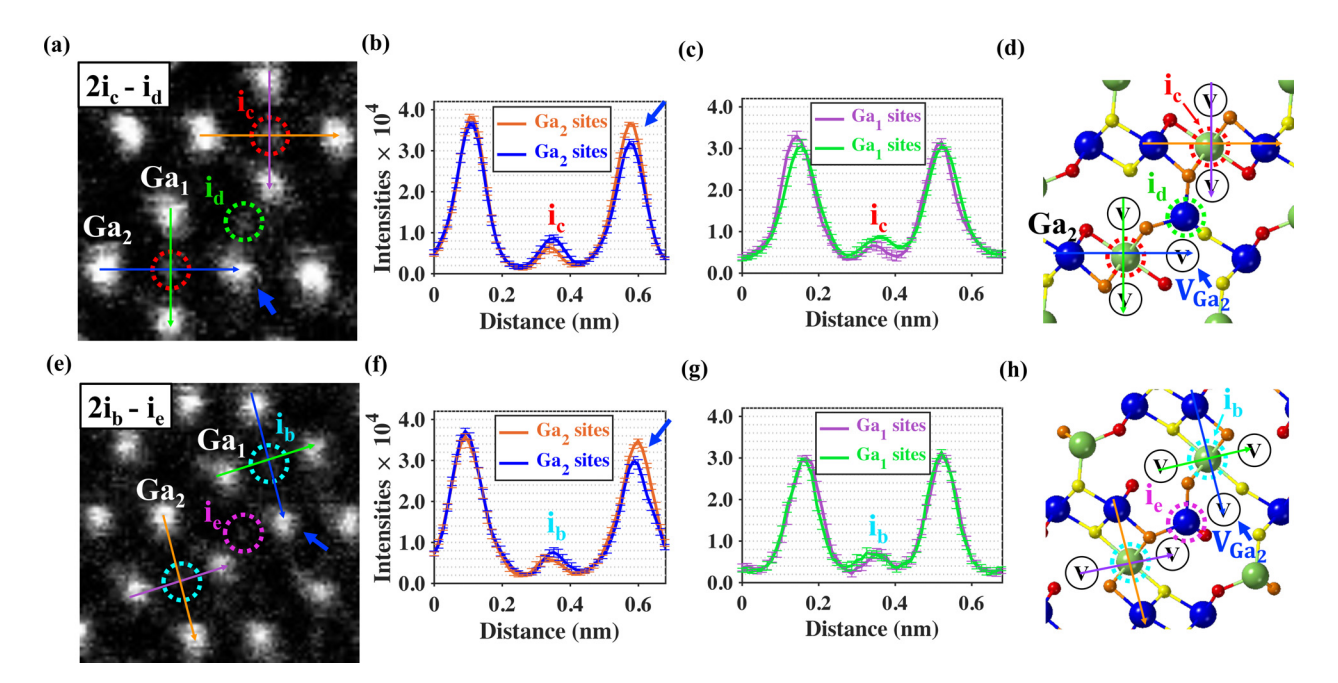


FIG. 2. (a) Experimental HAADF image of the region in Sn-doped β-Ga₂O₃ with two neighboring $2V_{Ga}^1$ -Ga_c^c complexes, with the positions of expected cation vacancies (indicated with a blue arrow) according to the formation mechanism of $2i_c$ - i_d complexes. (b) and (c) Line profile intensities across the same-colored lines in the image (a). The relatively low intensity of the right Ga₂ column (blue arrow) of the blue line confirms the higher concentration of vacancies in that column. The column intensities in (c) are lower than those of defect-free columns [orange line in (b)], indicating Ga₁ columns containing vacancies across both green and purple lines in (c). (d) The atomic model of the corresponding area in (a), reveals the vacancies (circles with V) occupying Ga₁ and Ga₂ columns (blue arrow). (e)–(h) Similar analysis of cation column intensities for the formation of $2i_b$ – i_e complexes.

presence of the V^1_{Ga} causes the neighboring Ga_1 atom to migrate into the interstitial site $(i_{b,c})$ which is located halfway between the two Ga_1 sites. Here, we show the proposed sequence of the formation of $2i_c\text{-}i_d$ [Figs. 3(a)-3(d)] and $2i_b\text{-}i_e$ [Figs. 3(e)-3(h)]]. For $2i_c\text{-}i_d$, when two adjacent i_c sites are occupied [Fig. 3(a)], which is likely to occur when the point defect concentration is high due to their clustering, two $2V^1_{Ga}\text{-}Ga^c_i$ complexes would form adjacent to each other [Fig. 3(b)]. From here, the fact that we observe both the i_d atom and V^2_{Ga} suggest that it is likely that the Ga atom originally sitting at the V^2_{Ga} position jumps to the i_d site (blue arrow from the lower V^2_{Ga} to the i_d site

above), resulting in the formation of $2i_c$ - i_d complex structures [Fig. 3(c)]. An alternative relaxation of the Ga_2 atom is also possible (blue arrow from the upper V_{Ga}^2 to the i_d site below) based on the site symmetry of the β - Ga_2O_3 unit cell. Therefore, each i_d site in Fig. 3(c) should have an equal probability of 50% occupancy. Figure 3(c) shows the structure combining the two cases, with the i_d site occupancy of 50% represented by the split color of the atom (aqua/white). This results in the creation of the structural motif outlined with the red-dotted line in Fig. 3(d). Similarly, an equivalent mechanism is also suggested for $2i_b$ - i_e and shown in Figs. 3(e)-3(h).

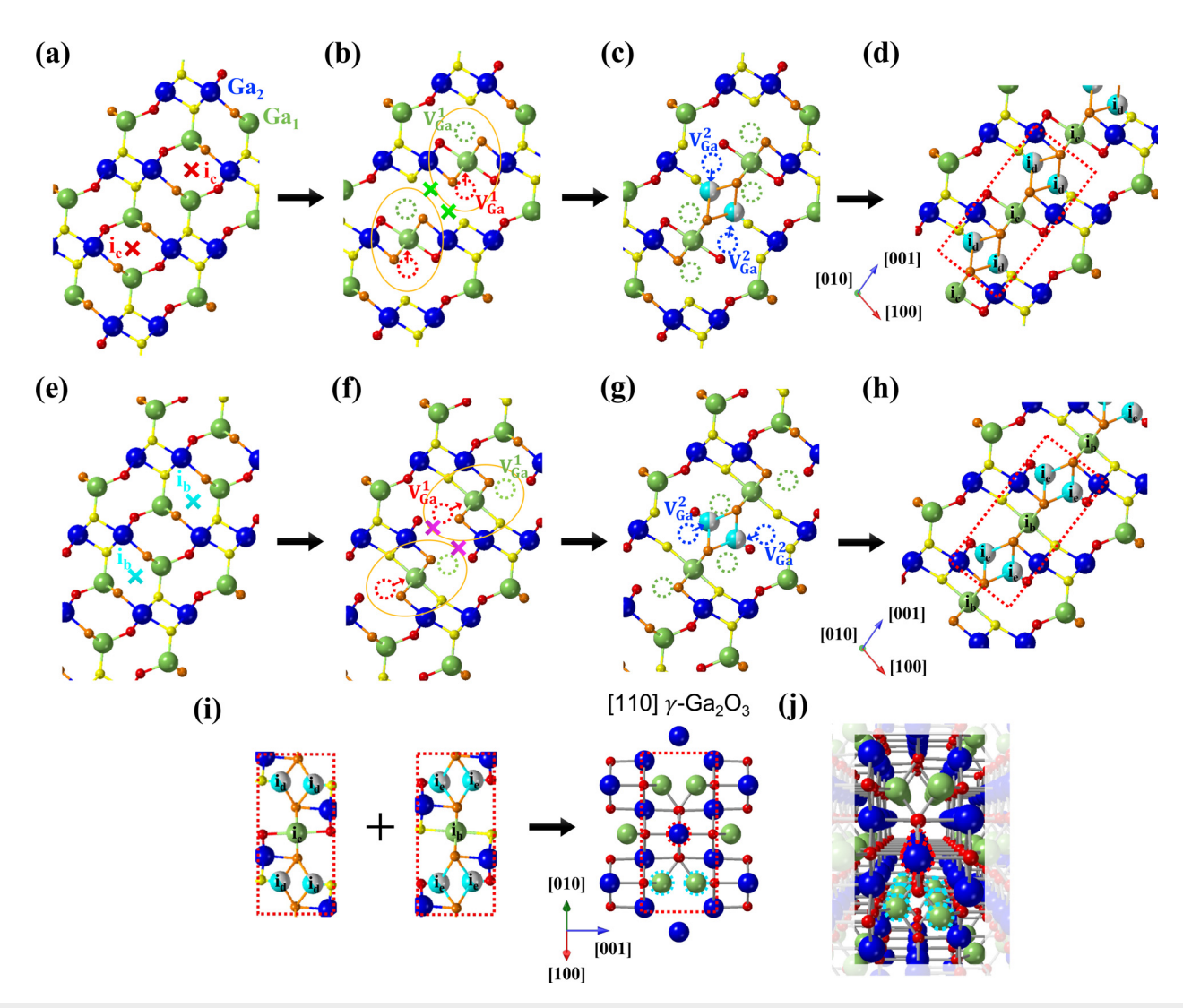


FIG. 3. (a)–(d) Schematic representation of the proposed mechanism for the formation of $2i_c$ – i_d complexes based on the STEM data. (a) A perfect lattice showing the potential i_c and i_d positions. (b) The migration of the adjacent Ga_1 into the i_c site (red arrow) induced by a V_{Ga}^i (green dotted circle), leading to a creation of an additional V_{Ga}^i (red dotted circle). This results in the formation of $2V_{Ga}^i$ complex (yellow oval), and two of them can be adjacent to each other. Two i_d sites (green X) can be identified due to the site symmetry of β-Ga₂O₃ unit cell. In such a case, one Ga_2 atom relaxes into either the lower i_d site or the upper i_d site (blue arrows in c) creating a V_{Ga}^2 defect. (d) The localized clustering of $2i_c$ – i_d complex structures, with the colors of i_d atoms (aqua/white) representing the 50% chance of occupancy. (e)–(h) Schematic representation of the equivalent mechanism for the formation of $2i_b$ – i_e complexes. (i) Possible phase transformation mechanism of the γ phase inclusion composed of two complex structures shown in (d) and (h). The split interstitial configurations with a 50% chance of occupancy results in a smaller number of atoms in tetrahedral sites (indicated with light blue dotted circles) compared to octahedral sites (indicated with red dotted circles) in the [110] γ phase structure. (j) Perspective view of the structure presented in (i).

In fact, when the two structural motifs (red-dotted rectangles) in Figs. 3(d) and 3(h) are combined, it becomes very similar to γ -Ga₂O₃, as shown in Fig. 3(i). Because the occupancy of i_d and i_e atoms are 50% (atoms with aqua/white coloring), the combination of the two structures will end up having 50% less Ga1 atoms (tetrahedrally coordinated Ga atoms) at corresponding positions in γ-Ga₂O₃ (green atoms within the red-dotted line). This connects well with the fact that γ-Ga₂O₃ has 50% less Ga₁ atoms as compared to Ga₂ atoms, which results in the zig-zag arrangement of the Ga₁ atoms shown in Fig. 3(j) (green atoms with aqua-dotted outline). This transformation may also involve some strain, as the position of the i_d and i_e atoms in β -Ga₂O₃ and the corresponding Ga₁ atoms positions in γ-Ga₂O₃ are slightly different as shown in Fig. 3(i). This mechanism shows a case where the ic (or ib) atoms are adjacent to each other, which is more likely to occur when the formation of the interstitial-divacancy complex (e.g., 2V_{Ga}-Ga_i^c) is facilitated by either doping¹⁵ or Si implantation.⁷ Therefore, it also implies that defect clustering may facilitate the lattice structure of interstitial complexes to relax and transform to the γ phase at a higher concentration of point defects (or complexes).

Based on the result obtained, we provide further discussion of the influence of impurities on the formation of the interstitial complexes and the transformation to γ -Ga₂O₃. For Sn-doped β -Ga₂O₃, previous findings¹⁵ have demonstrated that high concentrations of Sn doping in β -Ga₂O₃ crystals not only act as a substitutional dopant¹³ but also facilitate the formation of the vacancy-interstitial complexes. Sn doping has been found to exhibit n-type behavior in β -Ga₂O₃ by acting as a shallow donor. 70,71 As the material becomes more n-type, the energy of Fermi level increases, leading to a decrease in the formation energy of cation vacancies. This implies that Sn doping promotes the formation of the compensating acceptor species, such as $2V_{Ga}^1$ -Ga $_i^{b,c}$ complexes, through an increase in vacancy concentration. In the case of Si implantation, the Si dopant can also act as shallow donors and contribute to the n-type conductivity of β -Ga₂O₃, which suggests that Si ion implantation may also stimulate the formation of the vacancyinterstitial complexes. However, the effect of knock-on damage induced by ion implantation can also create point defects, leading to the formation of vacancy-interstitial complexes. Furthermore, the formation of vacancy-interstitial complexes is associated with the strain accumulation. Recent report confirmed that the γ phase was observed in implantations ranging from 1014 to 1016 ions/cm2. This suggests that the phase transformation from γ to β phase Ga_2O_3 can result the accumulation of strain and/or the preference of γ-Ga₂O₃ over highly defective β -Ga₂O₃⁶³. Based on these findings, we hypothesize that through the impurity incorporation (doping or ion implantation), the formation of interstitial 2ic,b-ide defect complexes resulted from the creation of cation vacancies. To maintain the strained crystal structure with the high concentration of defect complexes, the atomic relaxation mechanism occurs and forms the structure of γ phase inclusions.

In summary, the atomic scale mechanism of β to γ phase transformation was investigated by STEM. We demonstrated the structure of $2i_{c,b}-i_{d,e}$ defect complexes, resulting from two adjacent interstitial—divacancy complexes, which lead to the structure of γ phase inclusions. The formation of interstitial complexes have been quantitatively validated through column intensity analysis, and we further develop the formation mechanism of defect complexes to γ phase inclusion using atomistic modeling of lattice relaxation. The phase transformation implies lattice relaxation may occur at a higher concentration of point

defects (or complexes). Our STEM analysis offers crucial information on point defect identification in electronic materials, which is essential to advance for future device applications.

See the supplementary material for multislice simulations (Fig. S1), illustrating defect complexes involving with Ga interstitials in Sn-doped β -Ga₂O₃ and offering a more detailed description of the case observed in Fig. 2.

We acknowledge the support by the Department of Defense, Air Force Office of Scientific Research GAME MURI Program (Grant No. FA9550-18-1-0479). We thank Chris G. Van de Walle and Joel B. Varley for the helpful discussion on gamma phase gallium oxide. This work was performed in part at the Cornell PARADIM Electron Microcopy Facility and The Ohio State University Center of Center for Electron Microscopy and Analysis.

AUTHOR DECLARATIONS Conflict of Interest

The authors have no conflicts to disclose.

Author Contributions

Hsien-Lien Huang: Conceptualization (equal); Data curation (lead); Formal analysis (lead); Investigation (lead); Methodology (lead); Software (lead); Validation (equal); Visualization (equal); Writing – original draft (lead); Writing – review & editing (lead). Jared M. Johnson: Conceptualization (supporting); Formal analysis (supporting); Investigation (supporting); Methodology (supporting); Validation (supporting); Visualization (supporting); Writing – original draft (supporting). Christopher Chae: Formal analysis (supporting); Methodology (supporting); Writing – review & editing (equal). Alexander Senckowski: Methodology (supporting); Validation (supporting). Man Hoi Wong: Investigation (supporting); Methodology (supporting); Resources (supporting); Validation (supporting). Jinwoo Hwang: Conceptualization (lead); Funding acquisition (lead); Project administration (lead); Resources (lead); Supervision (lead); Writing – review & editing (equal).

DATA AVAILABILITY

The data that support the findings of this study are available from the corresponding authors upon reasonable request.

REFERENCES

- ¹M. Higashiwaki, K. Sasaki, A. Kuramata, T. Masui, and S. Yamakoshi, Phys. Status Solidi A 211, 21 (2014).
- ²M. Higashiwaki, K. Sasaki, H. Murakami, Y. Kumagai, A. Koukitu, A. Kuramata, T. Masui, and S. Yamakoshi, Semicond. Sci. Technol. 31, 034001 (2016).
- ³M. Higashiwaki, H. Murakami, Y. Kumagai, and A. Kuramata, Jpn. J. Appl. Phys., Part 1 55, 1202A1 (2016).
- ⁴M. Higashiwaki, A. Kuramata, H. Murakami, and Y. Kumagai, J. Phys. D: Appl. Phys. **50**, 333002 (2017).
- ⁵M. A. Mastro, A. Kuramata, J. Calkins, J. Kim, F. Ren, and S. J. Pearton, ECS J. Solid State Sci. Technol. 6, P356 (2017).
- ⁶S. J. Pearton, J. Yang, P. H. Cary, F. Ren, J. Kim, M. J. Tadjer, and M. A. Mastro, Appl. Phys. Rev. 5, 011301 (2018).

- ⁷Y. Zhang, A. Neal, Z. Xia, C. Joishi, J. M. Johnson, Y. Zheng, S. Bajaj, M. Brenner, D. Dorsey, K. Chabak, G. Jessen, J. Hwang, S. Mou, J. P. Heremans, and S. Rajan, Appl. Phys. Lett. 112, 173502 (2018).
- ⁸S. Krishnamoorthy, Z. Xia, C. Joishi, Y. Zhang, J. McGlone, J. Johnson, M. Brenner, A. R. Arehart, J. Hwang, S. Lodha, and S. Rajan, Appl. Phys. Lett. 111, 023502 (2017).
- ⁹M. Higashiwaki, K. Sasaki, A. Kuramata, T. Masui, and S. Yamakoshi, Appl. Phys. Lett. 100, 013504 (2012).
- ¹⁰H. H. Tippins, Phys. Rev. **140**, A316 (1965).
- ¹¹N. Ueda, H. Hosono, R. Waseda, and H. Kawazoe, Appl. Phys. Lett. **70**, 3561 (1997).
- ¹²H. L. Huang, C. Chae, and J. Hwang, J. Appl. Phys. **131**, 190901 (2022).
- ¹³J. B. Varley, J. R. Weber, A. Janotti, and C. G. Van De Walle, Appl. Phys. Lett. 97, 142106 (2010).
- ¹⁴H. Peelaers, J. B. Varley, J. S. Speck, and C. G. Van De Walle, Appl. Phys. Lett. 112, 242101 (2018).
- ¹⁵J. M. Johnson, Z. Chen, J. B. Varley, C. M. Jackson, E. Farzana, Z. Zhang, A. R. Arehart, H. L. Huang, A. Genc, S. A. Ringel, C. G. Van De Walle, D. A. Muller, and J. Hwang, Phys. Rev. X 9, 041027 (2019).
- ¹⁶H. Hayashi, R. Huang, H. Ikeno, F. Oba, S. Yoshioka, I. Tanaka, and S. Sonoda, Appl. Phys. Lett. **89**, 181903 (2006).
- ¹⁷Q. Liu, D. Guo, K. Chen, Y. Su, S. Wang, P. Li, and W. Tang, J. Alloys Compd. 731, 1225 (2018).
- ¹⁸ A. Hassa, C. Wouters, M. Kneiss, D. Splith, C. Sturm, H. von Wenckstern, M. Albrecht, M. Lorenz, and M. Grundmann, J. Phys. D: Appl. Phys. 53, 485105 (2020).
- ¹⁹A. Pichorim, I. T. Neckel, A. J. A. de Oliveira, J. Varalda, and D. H. Mosca, Mater. Chem. Phys. 287, 126320 (2022).
- ²⁰M. Zinkevich, F. Miguel Morales, H. Nitsche, M. Ahrens, M. Rühle, and F. Aldinger, Int. J. Mater. Res. 95, 756 (2022).
- ²¹H. Hayashi, R. Huang, F. Oba, T. Hirayama, and I. Tanaka, J. Mater. Sci. 46, 4169 (2011).
- ²²H. Hayashi, R. Huang, F. Oba, T. Hirayama, and I. Tanaka, J. Mater. Res. 26, 578 (2011).
- ²³T. Oshima, T. Nakazono, A. Mukai, and A. Ohtomo, J. Cryst. Growth **359**, 60
- ²⁴T. Oshima, Y. Kato, E. Magome, E. Kobayashi, and K. Takahashi, Jpn. J. Appl. Phys., Part 1 58, 060910 (2019).
- 25 Y. Kato, M. Imura, Y. Nakayama, M. Takeguchi, and T. Oshima, Appl. Phys. Express 12, 065503 (2019).
- ²⁶S. Nakagomi and Y. Kokubun, J. Cryst. Growth **479**, 67 (2017).
- ²⁷T. Oshima, Y. Kato, M. Oda, T. Hitora, and M. Kasu, Appl. Phys. Express 10, 051104 (2017).
- ²⁸V. Gottschalch, S. Merker, S. Blaurock, M. Kneiß, U. Teschner, M. Grundmann, and H. Krautscheid, J. Cryst. Growth 510, 76 (2019).
- ²⁹R. Lorenzi, A. Paleari, N. V. Golubev, E. S. Ignat'Eva, V. N. Sigaev, M. Niederberger, and A. Lauria, J. Mater. Chem. C 3, 41 (2015).
- 30 M. Hirano, K. Sakoda, and Y. Hirose, J. Sol-Gel Sci. Technol. 77, 348 (2016).
- ³¹L. Cui, H. Wang, B. Xin, and G. Mao, Appl. Phys. A **123**, 1 (2017).
- ³²M. M. Ruan, L. X. Song, Z. Yang, Y. Teng, Q. S. Wang, and Y. Q. Wang, J. Mater. Chem. C 5, 7161 (2017).
- 33X. Zhang, Z. Zhang, J. Liang, Y. Zhou, Y. Tong, Y. Wang, and X. Wang, J. Mater. Chem. A 5, 9702 (2017).
- ³⁴ X. Zhang, Z. Zhang, H. Huang, Y. Wang, N. Tong, J. Lin, D. Liu, and X. Wang, Nanoscale 10, 21509 (2018).
- 35Z. Yang, L. X. Song, Y. Q. Wang, M. M. Ruan, Y. Teng, J. Xia, J. Yang, S. S. Chen, and F. Wang, J. Mater. Chem. A 6, 2914 (2018).
- 36Y. Takano, Y. Hayashi, J. Fukushima, and H. Takizawa, Adv. Powder Technol. 32, 860 (2021).
- ³⁷C. Otero Areán, A. L. Bellan, M. P. Mentruit, M. R. Delgado, and G. T. Palomino, Microporous Mesoporous Mater. 40, 35 (2000).
- 38 M. R. Delgado, C. Morterra, G. Cerrato, G. Magnacca, and C. Otero Areán, Langmuir 18, 10255 (2002).
- ³⁹M. Hegde, T. Wang, Z. L. Miskovic, and P. V. Radovanovic, Appl. Phys. Lett. 100, 141903 (2012).
- 40 L. Li, W. Wei, and M. Behrens, Solid State Sci. 14, 971 (2012).
- ⁴¹S. W. Kim, S. Iwamoto, and M. Inoue, Ceram. Int. 35, 1603 (2009).

- ⁴²H. Y. Playford, A. C. Hannon, M. G. Tucker, D. M. Dawson, S. E. Ashbrook, R. J. Kastiban, J. Sloan, and R. I. Walton, J. Phys. Chem. C 118, 16188 (2014).
- ⁴³S. Jin, X. Wang, X. Wang, M. Ju, S. Shen, W. Liang, Y. Zhao, Z. Feng, H. Y. Playford, R. I. Walton, and C. Li, J. Phys. Chem. C 119, 18221 (2015).
- ⁴⁴D. S. Cook, R. J. Kashtiban, K. Krambrock, G. M. de Lima, H. O. Stumpf, L. R. S. Lara, J. D. Ardisson, and R. I. Walton, <u>Materials</u> 12, 838 (2019).
- ⁴⁵P. Castro-Fernández, M. V. Blanco, R. Verel, E. Willinger, A. Fedorov, P. M. Abdala, and C. R. Müller, J. Phys. Chem. C 124, 20578 (2020).
- ⁴⁶R. Horie, H. Nishinaka, D. Tahara, and M. Yoshimoto, J. Alloys Compd. 851, 156927 (2021).
- ⁴⁷A. Bhuiyan, Z. Feng, J. M. Johnson, H. L. Huang, J. Sarker, M. Zhu, M. R. Karim, B. Mazumder, J. Hwang, and H. Zhao, APL Mater. 8, 031104 (2020).
- ⁴⁸J. M. Johnson, H. L. Huang, M. Wang, S. Mu, J. B. Varley, A. F. M. A. Uddin Bhuiyan, Z. Feng, N. K. Kalarickal, S. Rajan, H. Zhao, C. G. Van de Walle, and J. Hwang, APL Mater. 9, 051103 (2021).
- 49T. Chen and K. Tang, Appl. Phys. Lett. 90, 053104 (2007).
- ⁵⁰T. Wang, S. S. Farvid, M. Abulikemu, and P. V. Radovanovic, J. Am. Chem. Soc. **132**, 9250 (2010).
- ⁵¹A. Singhal and I. Lieberwirth, Mater. Lett. **161**, 112 (2015).
- 52 T. Yamanaka, Y. Hayashi, and H. Takizawa, Ultrason. Sonochem. 89, 106114 (2022).
- 53T. Wang and P. V. Radovanovic, Chem. Commun. 47, 7161 (2011).
- 54S. S. Farvid, T. Wang, and P. V. Radovanovic, J. Am. Chem. Soc. 133, 6711 (2011).
- 55H. Hayashi, R. Huang, F. Oba, T. Hirayama, and I. Tanaka, Appl. Phys. Lett. 101, 241906 (2012).
- ⁵⁶M. Mitome, S. Kohiki, T. Nagai, K. Kurashima, K. Kimoto, and Y. Bando, Cryst. Growth Des. 13, 3577 (2013).
- ⁵⁷A. Sharma, M. Varshney, H. J. Shin, K. H. Chae, and S. O. Won, RSC Adv. 7, 52543 (2017).
- ⁵⁸H. Y. Playford, A. C. Hannon, E. R. Barney, and R. I. Walton, Chemistry 19, 2803 (2013).
- 59S. Yoshioka, H. Hayashi, A. Kuwabara, F. Oba, K. Matsunaga, and I. Tanaka, J. Phys. Condens. Matter 19, 346211 (2007).
- ⁶⁰C. S. Chang, N. Tanen, V. Protasenko, T. J. Asel, S. Mou, H. G. Xing, D. Jena, and D. A. Muller, APL Mater. 9, 051119 (2021).
- ⁶¹P. Vogt, F. V. E. Hensling, K. Azizie, C. S. Chang, D. Turner, J. Park, J. P. McCandless, H. Paik, B. J. Bocklund, G. Hoffman, O. Bierwagen, D. Jena, H. G. Xing, S. Mou, D. A. Muller, S. L. Shang, Z. K. Liu, and D. G. Schlom, APL Mater. 9, 031101 (2021).
- ⁶²K. R. Gann, C. S. Chang, M. C. Chang, D. R. Sutherland, A. B. Connolly, D. A. Muller, R. B. Van Dover, and M. O. Thompson, Appl. Phys. Lett. **121**, 062102 (2022).
- ⁶³J. García-Fernández, S. B. Kjeldby, P. D. Nguyen, O. B. Karlsen, L. Vines, and Ø. Prytz, Appl. Phys. Lett. **121**, 191601 (2022).
- 64S. B. Kjeldby, A. Azarov, P. D. Nguyen, V. Venkatachalapathy, R. Mikšová, A. MacKová, A. Kuznetsov, O. Prytz, and L. Vines, J. Appl. Phys. 131, 125701 (2022).
- 65 I. Cora, Z. Fogarassy, R. Fornari, M. Bosi, A. Rečnik, and B. Pécz, Acta Mater. 183, 216 (2020).
- ⁶⁶A. Azarov, C. Bazioti, V. Venkatachalapathy, P. Vajeeston, E. Monakhov, and A. Kuznetsov, Phys. Rev. Lett. **128**, 015704 (2022).
- 67 A. Kyrtsos, M. Matsubara, and E. Bellotti, Phys. Rev. B **95**, 245202 (2017).
- ⁶⁸J. B. Varley, H. Peelaers, A. Janotti, and C. G. Van De Walle, J. Phys. Condens. Matter 23, 334212 (2011).
- ⁶⁹M. E. Ingebrigtsen, A. Y. Kuznetsov, B. G. Svensson, G. Alfieri, A. Mihaila, U. Badstübner, A. Perron, L. Vines, and J. B. Varley, <u>APL Mater.</u> 7, 022510 (2019).
- ⁷⁰A. Kuramata, K. Koshi, S. Watanabe, Y. Yamaoka, T. Masui, and S. Yamakoshi, Jpn. J. Appl. Phys., Part 1 55, 1202A2 (2016).
- ⁷¹S. C. Siah, R. E. Brandt, K. Lim, L. T. Schelhas, R. Jaramillo, M. D. Heinemann, D. Chua, J. Wright, J. D. Perkins, C. U. Segre, R. G. Gordon, M. F. Toney, and T. Buonassisi, Appl. Phys. Lett. 107, 252103 (2015).
- 72J. M. Lebeau, S. D. Findlay, L. J. Allen, and S. Stemmer, Phys. Rev. Lett. 100, 206101 (2008)
- 73 E. J. Kirkland, R. F. Loane, and J. Silcox, Ultramicroscopy 23, 77 (1987).
- 74 H.-L. Huang, C. Chae, J. M. Johnson, A. Senckowski, S. Sharma, U. Singisetti, M. H. Wong, and J. Hwang, "Atomic Scale Defect Formation and Phase Transformation in Si Implanted β-Ga₂O₃," APL Mater. 11(6), 061113 (2023).